

Unusual strategies for using indium gallium nitride grown on silicon (111) for solid-state lighting

Hoon-sik Kim^{a,1}, Eric Brueckner^{b,1}, Jizhou Song^{c,1}, Yuhang Li^{d,e}, Seok Kim^a, Chaofeng Lu^{d,f}, Joshua Sulkin^g, Kent Choquette^g, Yonggang Huang^d, Ralph G. Nuzzo^{a,b,2}, and John A. Rogers^{a,b,g,2}

^aDepartment of Materials Science and Engineering, Frederick Seitz Materials Research Laboratory, Micro and Nanotechnology Laboratory, University of Illinois, 1304 West Green Street, Urbana, IL 61801; ^bDepartment of Chemistry, Frederick Seitz Materials Research Laboratory, Micro and Nanotechnology Laboratory, University of Illinois, 505 South Matthews Avenue, Urbana, IL 61801; ^cDepartment of Mechanical and Aerospace Engineering, University of Miami, Coral Gables, FL 33146; ^dDepartment of Civil and Environmental Engineering and Mechanical Engineering, Northwestern University, Evanston, IL 60208; ^eSchool of Astronautics, Harbin Institute of Technology, 92 West Dazhi Street, Harbin 150001, China; ^fSoft Matter Research Center and Department of Civil Engineering, Zhejiang University, 38 Zheda Road, Hangzhou 310027, China; and ^gDepartment of Electrical and Computer Engineering, Micro and Nanotechnology Laboratory, University of Illinois, 1406 West Green Street, Urbana, IL 61801

Edited by George M. Whitesides, Harvard University, Cambridge, MA, and approved May 10, 2011 (received for review February 16, 2011)

Properties that can now be achieved with advanced, blue indium gallium nitride light emitting diodes (LEDs) lead to their potential as replacements for existing infrastructure in general illumination, with important implications for efficient use of energy. Further advances in this technology will benefit from reexamination of the modes for incorporating this materials technology into lighting modules that manage light conversion, extraction, and distribution, in ways that minimize adverse thermal effects associated with operation, with packages that exploit the unique aspects of these light sources. We present here ideas in anisotropic etching, microscale device assembly/integration, and module configuration that address these challenges in unconventional ways. Various device demonstrations provide examples of the capabilities, including thin, flexible lighting “tapes” based on patterned phosphors and large collections of small light emitters on plastic substrates. Quantitative modeling and experimental evaluation of heat flow in such structures illustrates one particular, important aspect of their operation: small, distributed LEDs can be passively cooled simply by direct thermal transport through thin-film metallization used for electrical interconnect, providing an enhanced and scalable means to integrate these devices in modules for white light generation.

gallium nitride | solid-state lighting | transfer printing

Indium gallium nitride-based (InGaN) blue light emitting diodes (LEDs) hold a dominant position in the rapidly growing solid-state lighting industry (1, 2). The materials and designs for the active components of these devices are increasingly well developed due to widespread research focus on these aspects over the last one and a half decades. Internal and external quantum efficiencies of greater than 70% (3) and 60% (3), respectively, with luminous efficacies larger than 200 lm/W (4) and lifetimes of >50,000 h (5) are now possible. The efficacies (i.e., 249 lm/W), exceed those of triphosphor fluorescent lamps (i.e., 90lm/W), thereby making this technology an appealing choice for energy-efficient lighting systems (4). In particular, electricity consumption for lighting potentially could be cut in half using solid-state lighting (2). Although there remain opportunities for further improvements in these parameters, the emergence of LEDs into a ubiquitous technology for general illumination will rely critically on cost effective techniques for integrating the active materials into device packages, interconnecting them into modules, managing the accumulation of heat during their operation, and spatially homogenizing their light output at desired levels of chromaticity. Existing commercial methods use sophisticated, high-speed tools, but which are based on conceptually old procedures that exploit robotic systems to assemble material mechanically diced from a source wafer, with collections of bulk wires, lenses, and heat sinks in millimeter-scale packages, on a device-by-device basis, followed by separate steps to form

integrated lighting modules (6). The intrinsic features of such processes prohibit cost competitive realization of some of the most appealing configurations of LEDs for lighting, such as those that involve large collections of ultrasmall, thin devices distributed uniformly, but sparsely, over emissive areas of large modules that could serve as direct replacements for troffers currently used in fluorescent building lights. Alternative techniques, such as those that use directed assembly of solution suspensions of LEDs, first reported nearly twenty years ago (7), appear interesting, but efforts to design commercially relevant manufacturing schemes have been unsuccessful. Here we describe a set of procedures that aims to address the limitations of existing approaches in a different way, using ideas that extend our recent work in flexible electronics (8), information display (9), and photo-voltaics (10, 11), to the area of solid-state lighting by introducing new materials, etching strategies, interconnection methods, thermal management techniques, and schemes for wavelength conversion and light distribution. The process begins with removal of InGaN epitaxial material grown on silicon wafers with (111) orientation, using lithographically defined structures and anisotropic wet chemical etching, in ways that bypass conventional laser lift-off techniques and wafer dicing. When implemented with fully formed LEDs, these ideas can be combined with deterministic assembly via transfer printing (12) to allow high-throughput manipulation of devices with geometries that are orders of magnitude smaller than those compatible with robotic pick-and-place procedures. Self-aligned techniques for thin-film metallization that exploit the large band-gap of GaN provide remarkably simple routes to interconnect large collections of devices. The outcome consists of finely distributed sources of illumination that naturally manage the thermal aspects of operation through dramatically accelerated rates for passive heat spreading, consistent with analytical models for heat flow. Laminating such systems with patterned layers of phosphors and film-type optical diffusers yields thin, flexible lighting modules whose formats make them attractive for wide ranging applications in general illumination, both conventional and unconventional.

Author contributions: H.-S.K., E.B., R.G.N., and J.A.R. designed research; H.-S.K., E.B., J. Song, Y.L., S.K., C.L., and J. Sulkin performed research; R.G.N. and J.A.R. contributed new reagents/analytic tools; H.-S.K., E.B., J. Song, Y.L., S.K., K.C., Y.H., R.G.N., and J.A.R. analyzed data; and H.-S.K., E.B., J. Song, Y.H., R.G.N., and J.A.R. wrote the paper.

The authors declare no conflict of interest.

This article is a PNAS Direct Submission.

¹H.-S.K., E.B., and J. Song contributed equally to this work.

²To whom correspondence should be addressed. E-mail: r-nuzzo@illinois.edu or jrogers@illinois.edu.

This article contains supporting information online at www.pnas.org/lookup/suppl/doi:10.1073/pnas.1102650108/-DCSupplemental.

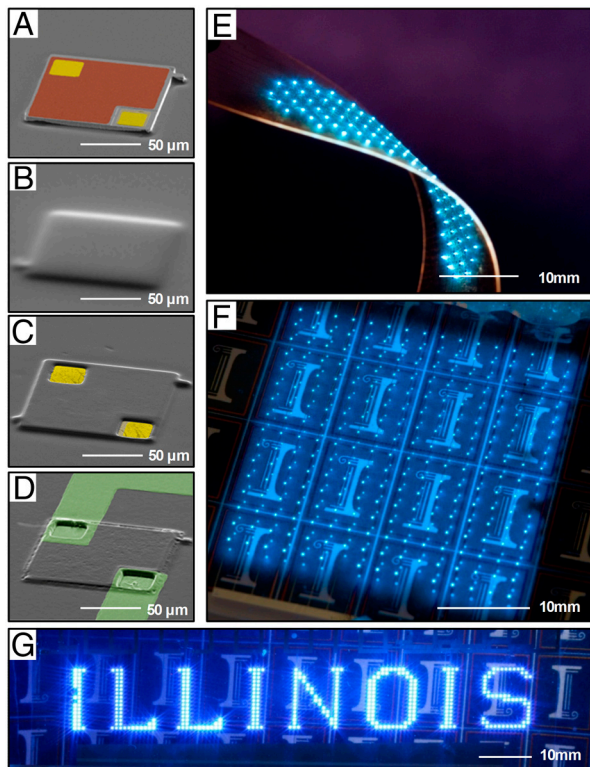


Fig. 2. SEM images of the interconnection process for a representative InGaN μ -LED, shown in sequence, (A) after assembly onto a optically transparent substrate (e.g., glass or plastic), (B) after spin-coating a photo-sensitive polymer, (C) after self-aligned via formation using a BSE process, and (D) after deposition and patterning of a metallic interconnect layer. The colored regions correspond to the contact pads (gold), a thin current spreading layer (red), and Al interconnects (green). Optical images of various lighting modules based on arrays of μ -LEDs (E) plastic and (F, G) glass substrates.

the size of a contact pad to the size of an entire device. This improvement corresponds to a factor of four for the case considered here with $25 \times 25 \mu\text{m}^2$ contact pads, but could be as large as a factor of 20 with $5 \times 5 \mu\text{m}^2$ contact pads. As shown in Fig. 2D, we purposefully interconnected arrays with overly wide leads (which we find easily accommodates small misalignments in the printed location of devices) by edge-over metallization, photolithographic patterning, and subsequent metal etching. This method is amenable to interconnecting large numbers of μ -LEDs over large area arrays (e.g., 396 μ -LEDs over $\sim 12 \text{ cm}^2$ in Fig. 2G), shown here for arrays integrated on polyethylene terephthalate (PET) (Fig. 2E) and on glass (Fig. 2F and G) substrates, and for exceptionally small devices. As an example of the latter capability, we could easily form vias of $\sim 4 \times 4 \mu\text{m}^2$ on devices with lateral dimensions as small as $25 \times 25 \mu\text{m}^2$ (Fig. S5D).

To illustrate the versatility, Fig. 3A–D show SEM images of exemplary μ -ILEDs with various sizes from (A) $25 \times 25 \mu\text{m}^2$, (B) $50 \times 50 \mu\text{m}^2$, (C) $75 \times 75 \mu\text{m}^2$, and (D) $150 \times 150 \mu\text{m}^2$. The sizes of the smallest and largest devices are limited by the resolution in device processing (i.e., lithography and mesa etching) and by degradation of etch-resist layers during silicon etching, respectively. The current density-voltage (J - V) characteristics of these μ -ILEDs show a noticeable increase in J as the size of μ -ILEDs decreases (Fig. 3E). This behavior might be attributed to superior current spreading in small devices (18). The properties are unaltered by the processing, as shown in Fig. 3F. The small, thin geometries also provide enhanced mechanical bendability (Fig. S6) (19) and dramatically improved rates for passive thermal spreading. Both of these qualities facilitate integration with

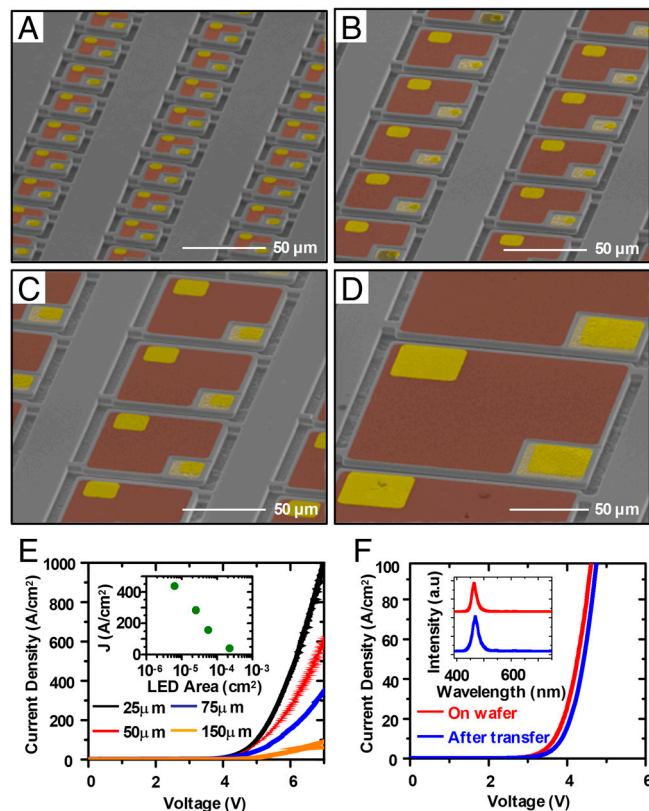


Fig. 3. SEM images of arrays of released InGaN μ -ILEDs with dimensions from (A) $25 \times 25 \mu\text{m}^2$, (B) $50 \times 50 \mu\text{m}^2$, (C) $75 \times 75 \mu\text{m}^2$ to (D) $150 \times 150 \mu\text{m}^2$. The colored regions correspond to the contact pads (gold), and thin current spreading layers (red). (E) Corresponding current density-voltage (J - V) characteristics for μ -ILEDs with the dimensions shown in (A). The inset provides a plot of current density as a function of μ -ILED area, measured at 6 V. (F) Current density-voltage (J - V) characteristics and emission spectrum (inset) of a representative device before undercut etching on the Si wafer, and after assembly onto a glass substrate.

flexible sheets of plastic, as shown in Fig. 2E. Details related to the bending mechanics appear in the *SI Text*; the thermal properties represent a focus of the *Discussion* section.

To demonstrate integrated sources of white light that exploit these unique capabilities, we developed schemes for integrating phosphors, patterned into small tiles, with arrays of μ -ILEDs and thin-film optical diffusers. As an example, we built a flexible lighting device that incorporates an amount of active material equal to that of a single, conventional $1 \times 1 \text{ mm}^2$ LED, but spread sparsely across an area of $\sim 300 \text{ mm}^2$ at an areal coverage corresponding to $\sim 0.3\%$ to optimize the thermal and optical properties (Fig. 4, Fig. S7). The process for constructing these systems follows two parallel routes: (i), μ -ILED fabrication, array assembly, and interconnection as shown in Fig. S2 using a thin, PET substrate similar to the one in Fig. 2, but with interconnects patterned such that 90% of each device is covered by reflective metal (Ti:3 nm/Al:500 nm), and the remaining 10% comprises the separation of leads to the p- and n- contacts; and, (ii), generation of a separate, patterned array of phosphor tiles matching the spatial geometry of the printed devices, on a soft, flexible sheet of the elastomer poly(dimethylsiloxane) (PDMS). The design of this second submodule is important because it allows the use of phosphor only where required, i.e., directly above each of the μ -ILEDs in the array. A schematic representation of the processing steps appears in Fig. 4A. The substrate consists of a thin sheet of PDMS embossed with an array of square wells of relief. A slurry incorporating a cerium-doped yttrium aluminum garnet phosphor (Intematix, NYAG-1) in an uncured PDMS matrix uniformly

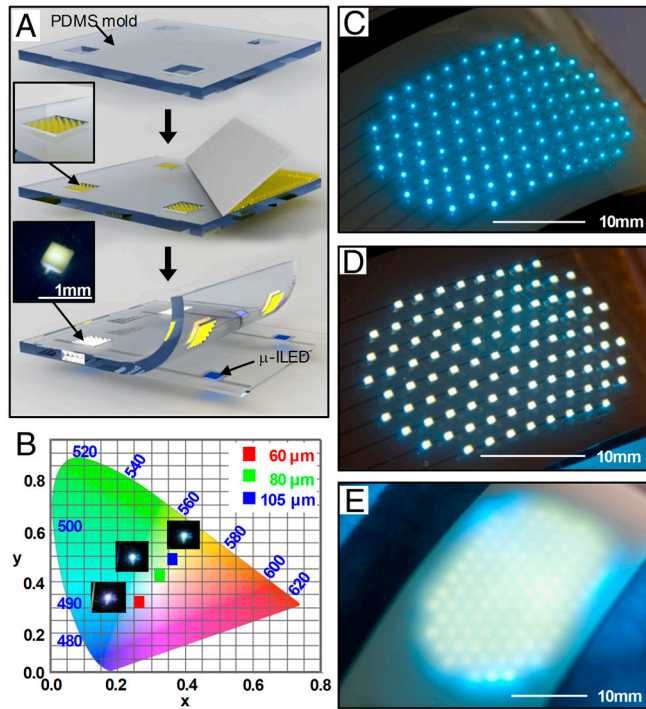


Fig. 4. (A) Schematic illustration of the process for fabricating flexible, white lighting modules, achieved by integrating patterned, encapsulated tiles of YAG:Ce phosphor islands with arrays of InGaN μ -ILEDs. (B) Color chromaticity plotted on a CIE 1931 color space diagram for μ -ILEDs integrated with phosphors with thicknesses of 60 μm , 80 μm , and 105 μm . Optical images of a fully interconnected array of μ -ILEDs (C) without phosphor, (D) with a laminated film of encapsulated YAG:Ce phosphor islands ($500 \times 500 \mu\text{m}^2$), and (E) with a laminated diffuser film.

disperses the phosphor particles (Fig. S8), in a manner that allows their delivery to the wells using a doctor blade. Thermally curing the slurry completes this part of the fabrication process. Soft contact lamination against a patterned, interconnected array of μ -ILEDs yields white light output, with chromaticity that can be tuned by controlling the well depth using slurries at a constant phosphor-in-PDMS weight loading (37.35 wt%). Chromaticity data at different phosphor thicknesses appear in an International Commission on Illumination (CIE) 1931 color space diagram in Fig. 4B. As expected, the chromaticity follows an approximately linear path between the limits of the blue emission of the μ -ILED and yellow emission of the phosphor with increasing thickness. For this PDMS-phosphor composition we obtain CIE coordinates of $x = 0.321$ and $y = 0.376$ with a phosphor thickness of 80 μm .

The LED component of the system consists of 100 μ -ILEDs, each $100 \times 100 \mu\text{m}^2$, in a hexagonal array, printed with an inter-device spacing of 2 mm, set to exceed the characteristic thermal diffusion length in this system. Fig. 4C and D shows images of the array before and after lamination against a sheet of patterned phosphor, respectively. (In this layout, the PET substrate provides a spacer between the μ -ILEDs and the phosphor tiles.) To complete the fabrication, a thin plastic diffuser film laminates onto the array to achieve diffuse, larger area emission, as in Fig. 4E. This sparse array of printed μ -ILEDs provides an effective illuminated area >100 times larger than the area of a traditional LED die, in a way that uses the same amount of InGaN in a configuration that has strong optical and thermal benefits.

Discussion

The thermal benefits of the type of layout in Fig. 4 are critically important, due to the adverse effects of excessive heating that can occur in devices with conventional sizes (e.g., $1 \times 1 \text{ mm}^2$) in the

absence of bulk, or miniature, heat sinking structures (20, 21). Quantitative study shows that for the sparse, μ -ILED designs, the electrical interconnects serve simultaneously as effective heat sinks. We examine the system using both analytical treatments and rigorous finite element methods (FEM) simulations. For the former, the approximately axi-symmetric nature of the system allows a precise analytical study of the thermal transport properties. The heat source is modeled as a disk with a radius r_0 , and total heat generation Q , which is approximately equal to the input power to the μ -ILED that does not result in light emission (22). The temperature distribution is obtained from the steady-state heat transfer governing equation $\frac{\partial^2 T}{\partial r^2} + \frac{1}{r} \frac{\partial T}{\partial r} + \frac{\partial^2 T}{\partial z^2} = 0$ in cylindrical coordinates (r, z) (Fig. S9). The boundary conditions include the free convection $-k_m \frac{dT}{dz} = h(T - T_\infty)$ at the top (air-interconnect) surface, and constant temperature $T = T_\infty$ at the bottom (glass) surface, where h is the coefficient of natural convection. The continuity of temperature and heat flux across the interconnect-BCB interface requires $[T] = 0$ and $[k \frac{dT}{dz}] = 0$, where $[\]$ stands for the discontinuity between two adjacent layers. The above continuity conditions also hold at other interfaces. Heat generation requires $[k \frac{\partial T}{\partial z}] = \frac{Q}{\pi r_0^2}$ ($r \leq r_0$) across the top and bottom surfaces of the μ -ILED. The interconnect surface temperature is obtained as (see SI Text for details)

$$T_{\text{surface}}(r) = T_\infty + \frac{Q}{2\pi r_0 k_b} \int_0^\infty [C_1(\xi) + C_2(\xi) e^{2\xi H_b}] e^{-\xi(H_b + H_m)} \times \frac{k_m}{k_m \xi + h} J_1(\xi r_0) J_0(\xi r) d\xi, \quad [1]$$

where

$$C_1(\xi) = (1 + k_b/k_m) \{ [(1 + k_g/k_b) - (1 - k_g/k_b) e^{2\xi(H_L + H_g)}] \beta(\xi) + 1 \},$$

$$C_2(\xi) = (1 - k_b/k_m) \{ [(1 - k_g/k_b) - (1 + k_g/k_b) e^{2\xi(H_L + H_g)}] \beta(\xi) - 1 \},$$

$$\beta(\xi) = (\kappa + 1) / \left\{ [(1 - k_g/k_b) - (1 + k_g/k_b) \kappa] - [(1 + k_g/k_b) - (1 - k_g/k_b) \kappa] e^{2\xi(H_L + H_g)} \right\},$$

$$\kappa = \left[\left(1 - \frac{k_b}{k_m} \right) - \frac{k_m \xi - h}{k_m \xi + h} \left(1 + \frac{k_b}{k_m} \right) e^{-2\xi H_m} \right] e^{-2\xi H_b} / \left[\frac{k_m \xi - h}{k_m \xi + h} \times \left(1 - \frac{k_b}{k_m} \right) e^{-2\xi H_m} - \left(1 + \frac{k_b}{k_m} \right) \right],$$

with J_0 and J_1 being the Bessel functions of order 0 and 1, respectively. The operating μ -ILED temperature is given by

$$T_{\text{LED}} = T_\infty + \frac{2Q}{k_b \pi r_0^2} \int_0^\infty (1 - e^{2\xi(H_L + H_g)}) \frac{\beta(\xi)}{\xi^2} J_1^2(\xi r_0) d\xi. \quad [2]$$

This analytical treatment agrees well with full three-dimensional FEM simulations as shown in Fig. S10D. The differences between temperatures in Eqs. 1 and 2 and FEM simulations are less than 3% for μ -ILED sizes from 10 μm to 100 μm with a 1,000 nm-thick interconnect at a power density 400 W/cm². The coefficient of natural convection is $h = 25 \text{ W/m}^2/\text{C}$ (23). Other conditions in experiments include the surrounding temperature $T_\infty = 50^\circ\text{C}$, thickness and thermal conductivity $H_b = 1 \mu\text{m}$, $k_b = 0.3 \text{ W/m}/\text{C}$ for BCB (24); $H_g = 800 \mu\text{m}$, $k_g = 1.1 \text{ W/m}/\text{C}$ for glass (25); and $H_L = 5 \mu\text{m}$ for μ -ILED. The thermal conductivity for Al interconnects is thickness dependent (26–29), and is taken as 70 W/m²/C and 160 W/m²/C for

300 nm-thick and 1,000 nm-thick interconnects, respectively. The radius of the disk heat source is $r_0 = 56 \mu\text{m}$ to yield the same area as the square $\mu\text{-ILED}$ with dimensions of $100 \times 100 \mu\text{m}^2$.

The left and right frames of Fig. 5 A–D show a set of experiments involving infrared thermal imaging of temperature distributions (QFI Infra-Scope Micro-Thermal Imager) and analytical predictions, respectively. These experiments compare surface temperatures for cases of Al interconnects with thicknesses of 300 nm and 1,000 nm (Fig. 5 A–B for 300 nm and Fig. 5 C–D for 1,000 nm), for input power ranging from 7.8 mW to 43.2 mW (i.e., power density ranging from 78 W/cm^2 to 432 W/cm^2). Fig. 5E presents surface temperatures as a function of power, where analytical model results (lines) agree very well the experimental measurements (symbols) for devices with these two interconnect thicknesses.

The results of Fig. 5 A–E clearly show pronounced decreases in the temperatures with thicker Al interconnects, thereby demonstrating that the interconnects themselves serve a dual role as efficient heat sinks by accelerating the rates of lateral thermal diffusion. These effects can be attributed predominantly to the significant thermal mass of the interconnects compared to the $\mu\text{-ILED}$ s, and to their higher thermal conductivities. As a consequence, both the thickness of the interconnects and the size of the devices are important. A theoretical parametric study, sum-

marized in Fig. 5F, shows the surface temperatures at a constant heat flux density of 400 W/cm^2 , as a function of these two variables. Clearly, the temperature can be greatly reduced by decreasing the sizes of the LEDs and by increasing the thicknesses of the interconnects. As a particular example, consider a conventional, macrosize LED (i.e., $1 \times 1 \text{ mm}^2$) and an array of 100 $\mu\text{-ILED}$ s (i.e., $100 \times 100 \mu\text{m}^2$) at a spacing of 2 mm on otherwise identical platforms, both at total input power densities of 400 W/cm^2 . The method of superposition is used to determine the temperature of $\mu\text{-ILED}$ arrays based on the solution for a single LED, i.e., $T_{\text{array}}(r,z) = T_{\infty} + \sum_i [T_i(r,z) - T_{\infty}]$, where $T_i(r,z)$ is the temperature distribution due to i th $\mu\text{-ILED}$. The surface temperature distributions for a macrosize LED and $\mu\text{-ILED}$ array with spacing 2 mm are shown in Fig. 5 G and H, respectively. The maximum temperature occurs at the center of the array and it decreases with increasing spacing (Fig. 5I). The conventional LED would reach a temperature of over $1,000^\circ\text{C}$ whereas the array of $\mu\text{-ILED}$ s would operate at $\sim 100^\circ\text{C}$ (Fig. S10D). In real devices, the conventional LED would be completely destroyed under these conditions, thereby motivating the requirement for advanced heat sinking structures of the type that are presently in use commercially. By contrast, the $\mu\text{-ILED}$ s experience temperatures that enable stable operation, without any additional components.

Conclusions

The strategies reported here incorporate advanced ideas in etching to release thin devices, self-aligned photoexposures to form metal features that serve simultaneously as electrical interconnects and thermal heat spreaders, and module designs that include thin, patterned phosphors with film diffusers. This collection of procedures, combined with analytical models of heat flow, create new design opportunities in solid-state lighting. Although all of these processes were combined to yield integrated systems, each can be implemented separately and matched to existing techniques for certain steps, to add new capabilities to otherwise conventional module designs. For example, the same concepts can be applied to active materials derived from epitaxial growth on sapphire substrates. These and other possibilities might represent interesting directions for future work.

Materials and Methods

Fabrication of GaN $\mu\text{-ILED}$ s. A GaN/Si(111) wafer (Azzurro Semiconductor) with layers of GaN:Mg (110 nm), five repeats of InGaN/GaN:Si (3 nm:10 nm), GaN:Si (1,700 nm), AlN:Si/GaN:Si (1,900 nm), GaN (750 nm), and AlN/AlGaIn (300 nm) served as the starting material. Multiple metal layers (Ti:15 nm/Al:60 nm/Mo:20 nm/Au:100 nm) are deposited via e-beam evaporator on regions of n-GaN exposed by ICP-RIE etching and annealed at 860°C for 30 s in N_2 ambient to form n-type ohmic contact to GaN:Si layer. For p-type ohmic contact to GaN:Mg layer, metal layers (Ni:10 nm/Au:10 nm) are deposited via e-beam evaporator and annealed at 500°C for 10 min in air ambient. Next, opaque contact pads are formed by e-beam evaporation (Ti:10 nm/Au:120 nm). As a resist for KOH attack on ohmic contacts, a 300 nm layer of silicon nitride was deposited by plasma enhanced chemical vapor deposition. The geometry of the device array was photo-lithographically defined by patterning a metal etch mask of metal (Ti:50 nm/Ni:450 nm) by photoresist lift-off process then removing the exposed silicon nitride by RIE with SF_6 . An ICP-RIE step provided the mesa etch, to generate an isolated array of devices. Anisotropic undercut etching of the silicon was performed by complete immersion in a solution of KOH (PSE-200, Transene) at 100°C (hot plate temperature).

Fabrication of Arrays of InGaN $\mu\text{-ILED}$ s. Devices were transfer printed from the source wafer to a target substrate, using procedures described elsewhere. BSE was performed by spin-casting and prebaking a layer of benzocyclobutene (Cyclotene 4024-40 Resin, 2,000 rpm for 60 sec, 80°C for 2 min). Samples were inverted, placed on a Cr-coated glass slide, exposed under a MJB3 Mask Aligner (Karl Suss), then developed (DS2100). After curing (210°C for 60 min in O_2 -free environment), interconnect metal (Ti/Al in desired thickness) was sputtered and patterned by photolithography and metal etching [Ti-6:1 BOE, Al-Al Etchant Type A (Transene)].

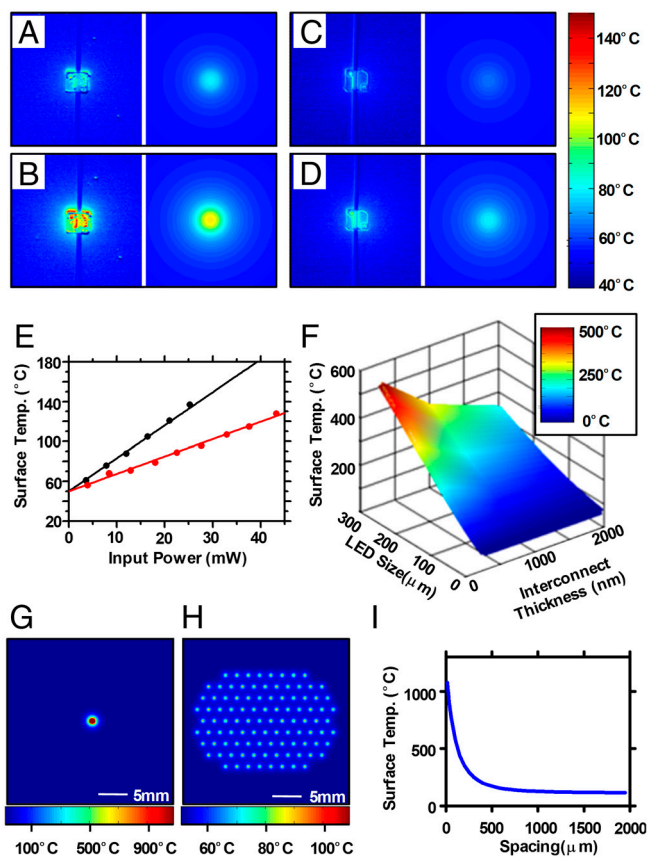


Fig. 5. (A–D) Temperature distributions for isolated InGaN $\mu\text{-ILED}$ s with Al interconnects [300 nm and 1,000 nm-thick for (A–B) and (C–D), respectively] at input powers of (A) 7.8 mW, (B) 16.4 mW, (C) 8.4 mW, and (D) 18.0 mW captured using a QFI Infra-Scope Micro-Thermal Imager (left) and calculated by analytical models (right). (E) Surface temperature for $\mu\text{-ILED}$ s with Al interconnect thicknesses of 300 nm (black) and 1,000 nm (red) extracted from experiments (dots) and computed using the analytical model (lines) as a function of input power. (F) Three-dimensional plot of the surface temperature as a function of device size and interconnect thickness, at a constant heat flux of 400 W/cm^2 . Temperature distribution for (G) a macrosize LED (i.e., $1 \times 1 \text{ mm}^2$), and (H) an array of 100 $\mu\text{-ILED}$ s (i.e., $100 \times 100 \mu\text{m}^2$) at a spacing of 2 mm. (I) $\mu\text{-ILED}$ s surface temperature vs. spacing for an array of 100 $\mu\text{-ILED}$ s.

Fabrication of Thin, Flexible, White Light Modules. Fabricating supports for the phosphor involved casting and curing PDMS (10:1 mixture of base to curing agent) against a functionalized silicon wafer (trichlorosilane, United Chemical Technologies) with a photodefined set of structures of epoxy (SU-8 50, MicroChem Corp.) with desired thicknesses. Peeling away the cured PDMS yielded an array of relief features ($500 \times 500 \mu\text{m}^2$) matching the spatial geometry of interconnected μ -LEDs. Phosphor islands were created by scraping a PDMS-based slurry of phosphor (NYAG-1, Intematix, created by mixing with uncured PDMS) across the PDMS substrate using a doctor-blade type implement consisting of a PDMS-coated razor blade. Thermal curing (70 °C for >3 h) completed the process. The phosphor mold was manually aligned and laminated to a matching array of μ -LEDs. The module was completed by bonding an optical diffuser film (AX27425, Anchor Optics) to the phosphor mold.

Characterization of Electrical, Optical, Mechanical, and Thermal Properties.

Electrical measurements were performed with a semiconductor parameter analyzer (4155C, Agilent or 2400 Sourcemeter, Keithley). Optical measurements of the emission spectra were performed with a high resolution spectrometer (HR4000, Ocean Optics). Color chromaticity was determined using SpectraSuite (Ocean Optics) with a radiometric calibration source (HL-2000,

Mikropack) and an Ocean Optics spectrometer optical fiber in a fixed location, ~ 1 mm, above the sample. Bending measurements involved determining the forward voltage needed to produce 10 mA current with the sample mounted on cylindrical tubes with various radii, ranging from 5.9 mm to 65.3 mm. Fatigue measurements were performed by repeatedly bending the specimen from a flat state to the bent state with a bending radius of 5.9 mm. Thermal measurements of the surface temperature of μ -LEDs were performed using MWIR-based InSb thermal imager (InfraScope, QFI) with the base temperature of 50 °C.

ACKNOWLEDGMENTS. We thank S. Elgan and N. Ahmed for help in transfer-printing using an automated printing tool. We also thank E. Chow for thermal imaging and L. Shi's help on the finite element modeling of the system. This material is based partly upon work supported by the Department of Energy, Division of Materials Sciences under Award No. DEFG02-91ER45439, through the Frederick Seitz MRL and Center for Microanalysis of Materials at the University of Illinois at Urbana-Champaign. For automated printers, the authors acknowledge the center for Nanoscale Chemical Electrical Mechanical Manufacturing Systems in University of Illinois, which is funded by National Science Foundation under grant DMI-0328162.

1. Tsao JY, Coltrin ME, Crawford MH, Simmons JA (2010) Solid-state lighting: an integrated human factors, technology, and economic perspective. *Proceedings of the IEEE* 98:1162–1179.
2. Schubert EF, Kim JK (2005) Solid-state light sources getting smart. *Science* 308:1274–1278.
3. Chen G, et al. (2008) Performance of high-power III-nitride light emitting diodes. *Physica Status Solidi (a)* 205:1086–1092.
4. Narukawa Y, Ichikawa M, Sanga D, Sano M, Mukai T (2010) White light emitting diodes with super-high luminous efficacy. *J Phys D Appl Phys* 43:354002.
5. US Department of Energy (2010) Solid-state lighting research and development: Multi-year program plan. (US DoE, Washington, DC), Available from <http://www1.eere.energy.gov/buildings/ssl/techroadmaps.html>.
6. Karlicek RF, Jr (2005) High power LED packaging. *Conference on Lasers and Electro-optics (CLEO)* (IEEE, MD), pp 337–339.
7. Yeh H-JJ, Smith JS (1994) Fluidic self-assembly for the integration of GaAs light-emitting diodes on Si substrates. *IEEE Photonic Tech L* 6:706–708.
8. Kim D-H, et al. (2008) Materials and noncoplanar mesh designs for integrated circuits with linear elastic responses to extreme mechanical deformations. *Proc Natl Acad Sci USA* 105:18675–18680.
9. Park S-I, et al. (2009) Printed assemblies of inorganic light-emitting diodes for deformable and semitransparent displays. *Science* 325:977–981.
10. Yoon J, et al. (2008) Ultrathin silicon solar microcells for semitransparent, mechanically flexible and microconcentrator module designs. *Nat Mater* 7:907–915.
11. Yoon J, et al. (2010) GaAs photovoltaics and optoelectronics using releasable multilayer epitaxial assemblies. *Nature* 465:329–334.
12. Meitl MA, et al. (2006) Transfer printing by kinetic control of adhesion to an elastomeric stamp. *Nat Mater* 5:33–38.
13. Lee J, et al. (2011) Growth of high-quality InGaN/GaN LED structures on (111) Si substrates with internal quantum efficiency exceeding 50%. *J Cryst Growth* 315:263–266.
14. Kumar V, Zhou L, Selvanathan D, Adesida I (2002) Thermally-stable low-resistance Ti/Al/Mo/Au multilayer ohmic contacts on n-GaN. *J Appl Phys* 92:1712–1714.
15. Baca AJ, et al. (2007) Printable single-crystal silicon micro/nanoscale ribbons, platelets and bars generated from bulk wafers. *Adv Funct Mater* 17:3051–3062.
16. Bean KE (1978) Anisotropic etching of silicon. *IEEE T Electron Dev* ED-25:1185–1193.
17. Kim R-H, et al. (2010) Waterproof AllnGaP optoelectronics on stretchable substrates with applications in biomedicine and robotics. *Nat Mater* 9:929–937.
18. Gong Z, et al. (2010) Size-dependent light output, spectral shift, and self-heating of 400 nm InGaN light-emitting diodes. *J Appl Phys* 107:013103.
19. Sou Z, Ma EY, Gleskova H, Wagner S (1999) Mechanics of rollable and foldable film-on-foil electronics. *Appl Phys Lett* 74:1177–1179.
20. Moon S-M, Kwak JS (2009) High-current electro-optical degradation of InGaN/GaN light-emitting diodes fabricated with Ag-based reflectors. *J Korean Phys Soc* 55:1128–1131.
21. Arik M, Weaver S (2004) Chip scale thermal management of high brightness LED packages. *P SPIE IS and T Elect Im* 5530:214–223.
22. Senawiratne J, et al. (2008) Junction temperature measurements and thermal modeling of GaInN/GaN quantum well light-emitting diodes. *J Electron Mater* 37:607–610.
23. Incropera FP, DeWitt DP, Bergman TL, Layine AS (2007) *Fundamentals of Heat and Mass Transfer* (Wiley, Hoboken), pp 6–9.
24. Christiaens I, Roelkens G, Mesel KD, Thourhout DV, Baets R (2005) Thin-film devices fabricated with benzocyclobutene adhesive wafer bonding. *J Lightwave Technol* 23:517–523.
25. Lee SM, Cahill G (1997) Heat transport in thin dielectric films. *J Appl Phys* 81:2590–2595.
26. Bourgoin J-P, Allogho G-G, Hache A (2010) Thermal conduction in thin films measured by optical surface thermal lensing. *J Appl Phys* 108:073520.
27. Schmidt AJ, Cheaito R, Chiesa M (2010) Characterization of thin metal films via frequency-domain thermoreflectance. *J Appl Phys* 107:024908.
28. Spina LL, et al. (2006) MEMS test structure for measuring thermal conductivity of thin films. *Proc IEEE International Conference on Microelectronic Test Structures* pp 137–142 Austin, TX.
29. Stojanovic N, et al. (2007) Thin-film thermal conductivity measurement using microelectrothermal test structures and finite-element-model-based data analysis. *J Microelectromech S* 16:1269–1275.